Figure 7 shows the functions $W(\gamma)$ calculated for a resonant H (full curve) and for a constant H (dotted curve). Also shown is the experimental histogram obtained[11] at a proton energy of 650 Mev. Although the statistics are not very good, it is clear from Fig. 7 that the experiment agrees better with a resonant than with a constant interaction.

The author thanks M. G. Meshcheriakov, B. S. Neganov, V. P. Zrelov, I. K. Vzorov, and A. F. Shabudin for information about their experimental results, and also L. M. Lapidus for valuable advice and criticism.

[1] K. Brueckner, Phys. Rev. **86**, 106 (1952).
[2] Tamm, Gol'fand and Fainberg, J. Exptl. Theoret. Phys. (U.S.S.R.) **26**, 649 (1954).
[3] D. C. Peaslee, Phys. Rev. **94**, 1085 (1954).
[4] S. Z. Belen'kii and A. I. Nikishov, J. Exptl. Theoret. Phys. (U.S.S.R.) **28**, 744 (1955); Soviet Phys. **1**, 593 (1955).
[5] Aitken, Mahmoud, Henley, Ruderman and Watson, Phys. Rev. **93**, 1349 (1954).
[6] M. Gell-Mann and K. M. Watson, Annual Rev. Nucl. Sci. **4**, 219 (1954).
[7] H. A. Bethe and F. DeHoffmann, *Mesons and Fields* [Row, Peterson (Evanston 1955)] Vol. **2**, 130.
[8] I. L. Rozental', J. Exptl. Theoret. Phys. (U.S.S.R.) **28**, 118 (1955); Soviet Phys. **1**, 166 (1955).
[9] Meshcheriakov, Zrelov, Neganov, Vzorov and Shabudin, J. Exptl. Theoret. Phys. (U.S.S.R.) **31**, 45 (1956); Soviet Phys. **4**, 60 (1957).
[10] Meshcheriakov, Neganov, Zrelov, Vzorov and Shabudin, Dokl. Akad. Nauk SSSR, **109**, 499 (1956); Soviet Phys. "Doklady," **1**, 447 (1957).
[11] L. Riddiford, *Proton-proton interaction at 650 Mev*, Report to Liverpool Conference (1955).
[12] F. E. Mills and L. J. Koester, Phys. Rev. **98**, 210 (1955).
[13] Watson, Keck, Tollestrup and Walker, Phys. Rev. **101**, 1159 (1956).
[14] Goldschmidt-Clermont, Osborne and Scott, Phys. Rev. **97**, 188 (1955).
[15] D. C. Oakley and R. L. Walker, Phys. Rev. **97**, 1283 (1955).

Translated by F. J. Dyson
232

SOVIET PHYSICS JETP VOLUME 5, NUMBER 5 DECEMBER, 1957

Model of a Semi-transparent Nucleus with a Diffuse Boundary, II

P. E. NEMIROVSKII

(Submitted to JETP editor June 12, 1956)
J. Exptl. Theoret. Phys. (U.S.S.R.) **32**, 1143-1149 (May, 1957)

A new method is presented for calculating nuclear interaction cross-sections for low energy neutrons. Assuming that no absorption occurs in the surface layer, it is shown that the energy dependence of the cross-section at low energy is the same for a potential with diffuse boundary as for a rectangular well. The capture cross-section is larger for the diffuse than for the sharp boundary. Values of the parameters and of the nuclear potential are found which give satisfactory agreement with experiment over a wide range of nuclear weights and energies.

IN AN EARLIER PAPER[1] we reported results of calculations of cross-sections for a semi-transparent nuclear model with diffuse boundary. We found good agreement of the capture of cross-sections transparent nuclear model with diffuse boundary. We found good agreement on the capture of cross-sections with experiment, up to an energy of a few million volts, with the following values of the parameters:

$$V(r) = 20\,\text{MeV} \quad \text{for} \quad r \leqslant r_0,$$

$$V(r) = 20 \exp\{-(r - r_0)/1.4 \cdot 10^{-13}\} \quad \text{for} \quad r \geqslant r_0,$$

$$r_0 + 1.4 \cdot 10^{-13} = 1.25 \cdot 10^{-13} A^{1/3}\ \text{cm}.$$

The imaginary part $\zeta V(r)$ of the potential was variable. However, it has since been reported[2] that the potential $V(r)$ should be 42 Mev. Also it seems appropriate to compare the calculated results with a

wider range of experimental data, in order to test the diffuse-boundary model and to choose the most satisfactory set of parameters to describe nuclear matter. Therefore we decided to carry out calculations of total cross-sections for the diffuse-boundary model at low energies. We found some devices which allow us to simplify the calculation to the point where numerical computations are avoided.

1. CALCULATION OF PHASE-SHIFT

Suppose $V = V(r_0)$ for $r \leq r_0$. A boundary condition must be satisfied at $r = r_0$. The internal wave-function at $r = r_0$ is evidently

$$\Psi_l^{(i)} = (\mathrm{X} + i\xi)^{-1/2} J_{l+1/2}(\mathrm{X} + i\xi), \qquad (1)$$

with $\mathrm{X} = K_0 r_0$, $\xi = \varkappa r_0$, where K and $\varkappa$ are the real and imaginary parts of the wave-number. We write

$$d \ln \Psi_l^{(i)}/d\mathrm{X} = (K/K_0) A_l. \qquad (2)$$

Then the boundary condition is

$$A_l = \frac{1}{\Psi_l^{(a)}} \frac{d\Psi_l^{(a)}}{dx} \quad \text{for} \quad r = r_0 \qquad (3)$$

where $x = kr$, and $X_l^{(a)}$ is the wave-function for $r \geq r_0$. But

$$\Psi_l^{(a)} = \Psi_l^{\mathrm{II}} + \eta_l \Psi_l^{\mathrm{I}},$$

where Ψ_l^{I} represents an outgoing wave at $x = \infty$, and Ψ_l^{II} an ingoing wave. Substituting (3a) into (3), we obtain

$$A_l = \left(\frac{d\Psi_l^{\mathrm{II}}}{dx} + \eta_l \frac{d\Psi_l^{\mathrm{I}}}{dx}\right) / (\Psi_l^{\mathrm{II}} + \eta_l \Psi_l^{\mathrm{I}}), \qquad (4)$$

and hence

$$\eta_l = \left(A_l \Psi_l^{\mathrm{II}} - \frac{d\Psi_l^{\mathrm{II}}}{dx}\right) \Big/ \left(\frac{d\Psi_l^{\mathrm{I}}}{dx} - A_l \Psi_l^{\mathrm{I}}\right) \qquad (5)$$

Obviously, Ψ_l^{I} and Ψ_l^{II} can be written in the form

$$\begin{aligned} \Psi_l^{\mathrm{I}} &= x^{-1/2} H_{l+1/2}^{(1)}(x)\, v_l^{(1)}(x), \ \Psi_l^{\mathrm{II}} \\ &= x^{-1/2} H_{l+1/2}^{(2)}(x)\, v_l^{(2)}(x), \end{aligned} \qquad (6)$$

with $v_l^{(1)} = v_l^{(2)} = 1$ for $x \to \infty$. From Eqs. (6) and (5) we obtain

$$\eta_l = \frac{x^{1/2} v_l^{(2)} H_{l+1/2}^{(2)}(x) \left[A_l - \frac{1}{v_l^{(2)}} \frac{dv_l^{(2)}}{dx} - \frac{d \ln x^{1/2} H_{l+1/2}^{(2)}}{dx}\right]}{x^{1/2} v_l^{(1)} H_{l+1/2}^{(1)}(x) \left[\frac{1}{v_l^{(1)}} \frac{dv_l^{(1)}}{dx} - A_l + \frac{d \ln x^{1/2} H_{l+1/2}^{(1)}}{dx}\right]}. \qquad (7)$$

Introducing

$$S_l^{(2)} = d \ln v_l^{(2)}/dx, \quad S_l^{(1)} = d \ln v_l^{(1)}/dx,$$

$$f_l = d \ln x^{1/2} H_{l+1/2}^{(1)}/dx,$$

we find

$$\frac{\sigma_a^{(l)}}{(2l+1)\pi\lambda^2} = 1 - |\eta_l|^2 = 1 - \frac{|v_l^{(2)}|^2 |A_l - S_l^{(2)} - f_l^*|^2}{|v_l^{(1)}|^2 |A_l - S_l^{(1)} - f_l|^2}, \qquad (8)$$

$$\frac{\sigma_e^{(l)}}{(2l+1)\pi\lambda^2} = |1 - \eta_l|^2 = \left|1 + \frac{H_{l+1/2}^{(2)}(x)\, v_l^{(2)} (A_l - S_l^{(2)} - f_l^*)}{H_{l+1/2}^{(1)}(x)\, v_l^{(1)} (A_l - S_l^{(1)} - f_l)}\right|^2. \qquad (9)$$

When $v_l^{(2)} = v_l^{(1)} = 1$ and $S_l^{(2)} = S_l^{(1)} = 0$, Eqs. (8) and (9) reduce to the formulas for a sharp boundary.

The case in which $V(r)$ is real for $r \geq r_0$ is particularly simple. Then $v_l^{(2)} = v_l^{(1)} = v_l$,

$$1 - |\eta_l|^2 = -\frac{4 \operatorname{Im} A_l [\operatorname{Im} S_l + h_l]}{|A_l - S_l - f_l|^2}, \qquad (10)$$

$$|1 - \eta_l|^2 = \left|1 + e^{-2i\psi - 2i\varphi} \frac{A_l - S_l^* - f_l^*}{A_l - S_l - f_l}\right|^2, \qquad (11)$$

$$\begin{aligned} f_l &= g_l + ih_l, \ v_l = |v_l| e^{-i\varphi}, \\ H_{l+1/2}^{(2)} &= |H_{l+1/2}^{(2)}| e^{-i\psi}. \end{aligned} \qquad (12)$$

The function S_l satisfies the equation

$$dS_l/dx + S_l^2 + 2f_l S_l + (K_0/k)^2 V(x) = 0, \qquad (13)$$

with $V(x_0) = 1$. Separating the real and imaginary parts $S_l = a_l + ib_l$ in Eq. (13), we have

$$\frac{da_l}{dx} + a_l^2 - b_l^2 + 2g_l(x)\, a_l - 2h_l(x)\, b_l + \frac{K_0^2}{K^2} V(x) = 0 \qquad (14a)$$

$$\frac{db_l}{dx} + 2a_l b_l + 2g_l(x)\, b_l + 2h_l(x)\, a_l = 0. \qquad (14b)$$

By means of Eq. (14b) we can express b_l in terms of a_l. The Hankel functions satisfy here the identity

$$2\int_x^\infty g_l(x')\,dx' = \ln h_l(x).$$

Hence the general solution of the homogeneous part of Eq. (14b) is

$$b_l = Ch_l(x)\exp\left(2\int_x^\infty a_l(x')\,dx'\right),$$

and the solution of the inhomogeneous equation is

$$b_l = h_l\exp\left\{2\int_x^\infty a_l(x')\,dx'\right\} \times\int_x^\infty \exp\left\{-2\int_x^\infty a_l(x'')\,dx''\right\} 2a_l(x')\,dx'.$$

which reduces to

$$b_l = h_l(x)\left[\exp\left(2\int_x^\infty a_l(x')\,dx'\right) - 1\right]. \qquad (15)$$

Thus Eq. (10) can be written

$$1 - |\eta_{lt}|^2 = -\frac{4\,\mathrm{Im}\,A_l h_l \exp\left\{2\int_x^\infty a_l(x')\,dx'\right\}}{[\mathrm{Re}\,A_l - a_l - g_l(x)]^2 + \left[\mathrm{Im}\,A_l - h_l\exp\left\{2\int_x^\infty a_l(x')\,dx'\right\}\right]^2} \qquad (16)$$

and a similar expression holds for $|1-\eta_l|^2$.

At low energy, the quantities b_l^2 and $h_l b_l$ are small and Eq. (14a) can be solved independently of (14b). The resulting value of a_l can then be used to determine b_l.

The function $\exp\left\{2\int_x^\infty a_l\,dx\right\}$ varies slowly with radius and with energy. Hence we can interpolate between values of the function calculated at the ends of a wide interval. The main energy-dependence of the cross-section comes from the factor $h_l(x)$, which is a known rational function of the energy. Also at low energy, when $kr_0 < l$, the capture cross-section becomes proportional to x^{2l-1}, as for a rectangular well. But it may happen that the capture cross-section for a diffuse boundary is greater than for a rectangular well with the same depth and coefficient of absorption.

2. COMPARISON WITH EXPERIMENT

Detailed calculations of cross-sections were made with a boundary of exponential shape. With a well-depth $V(0) = 45$ Mev and a boundary shape $e^{-\alpha(r-r_0)}$ where $1/\alpha = 1\times10^{-13}$ cm, the calculated total cross-sections at 1 Mev were much larger than the experimental values, and had too sharp maxima as functions of r_0. The imaginary part of the potential was taken to be $0.03\,V(r)$. The calculated cross-sections $\sigma_t(r_0)$ and $\sigma_a(r_0)$ are shown graphically in Figs. 1 and 2. Consequently the later calculations were made with the value $\alpha = K_0 = 1.43\times10^{13}$ cm^{-1}.

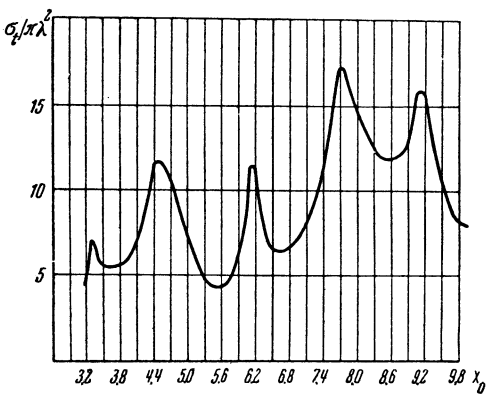

FIG. 1. Total cross-section as a function of r_0 for neutron energy 1 Mev. Parameters $1/\alpha = 10^{-13}$ cm, $\zeta = 0.03$.

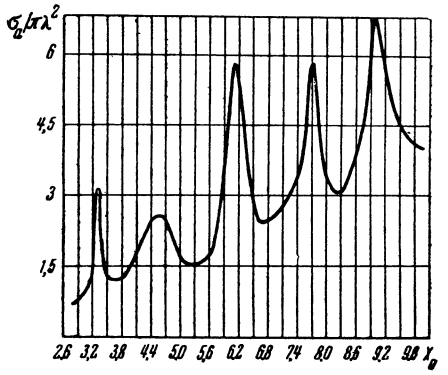

FIG. 2. Capture cross-section as a function of r_0 for neutron energy 1 Mev. Parameters $1/\alpha = 10^{-13}$ cm, $\zeta = 0.03$.

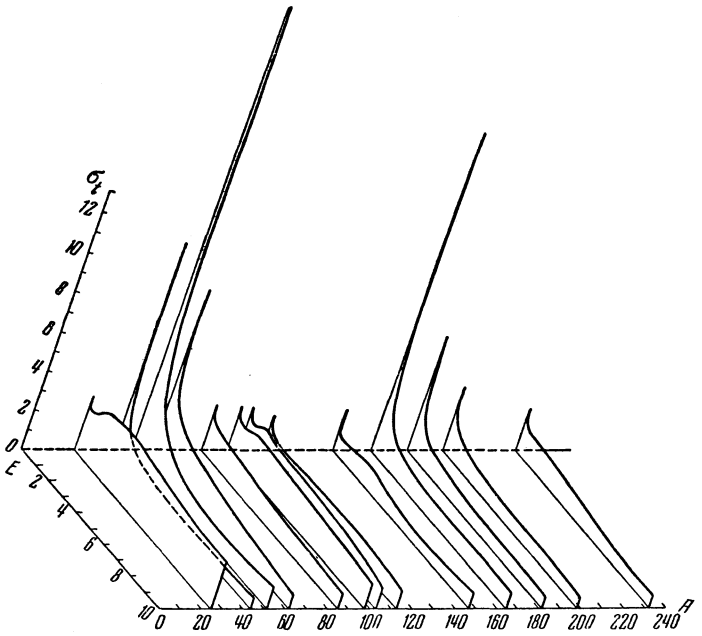

FIG. 3. Total nuclear cross-sections. The x axis represents atomic weight, the y axis neutron energy in units of 0.1 Mev, the z axis $\sigma_t/\pi R^2$.

With this value of α we constructed surfaces showing the total cross-section as a function of energy and atomic weight (see Fig. 3). The imaginary fraction of the potential was taken to be 0.05 for $r \leq r_0$ and zero for $r \geq r_0$. The calculations with $1/\alpha = 1 \times 10^{-13}$ cm had shown that the vanishing of the imaginary part of the potential in the surface layer did not significantly change the behavior of the cross-sections.

Satisfactory agreement with experiment was found with $V(0) = 44$ Mev and $r_0 = 1.25 \times 10^{-13} A^{1/3}$ cm. The minimum of the cross-section at 1 Mev for elements with $A \sim 200$ is clearly visible, as is the maximum for elements with $A \sim 90$–100. The maximum at 1 Mev in the region of titanium is apparently missing, and the cross-sections for $A = 150$–180 are bigger and less energy-dependent than the theoretical values. The latter discrepancy is probably connected with the non-spherical shapes of nuclei in this region.

Capture cross-sections were also calculated at various energies. Unfortunately the experimental data at 1 Mev (see Fig. 4) are inconclusive. Elastic scattering through compound nucleus states is small for silver and gold, and $\sigma_a \sim 2$ barns. The theory gives 2 barns for gold and 1.7 for silver. For iron the capture cross-section is probably greater than 1 barn, since the scattering into the spin-2 level at 860 kev is 0.4 barn and the compound nucleus decays predominantly into the elastic channel. The theory gives 1.8 barns for iron. Thus there is no contradiction with experiment.

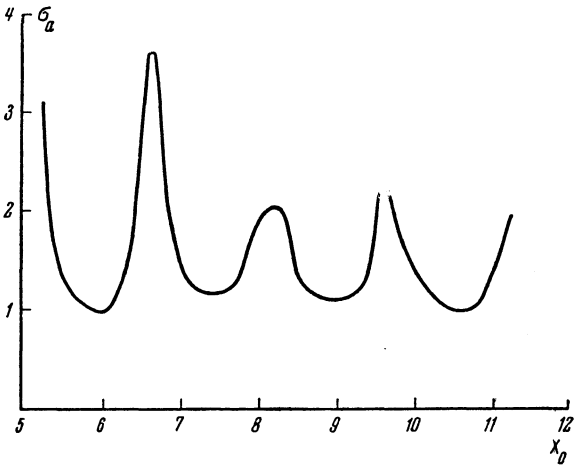

FIG. 4. Neutron capture cross-section in units of $\pi(r_0 + 1/\alpha)^2$ as a function of r_0 for energy 1 Mev. Parameters $1/\alpha = 0.71 \times 10^{-13}$ cm, $\zeta = 0.05$.

At low energy one can compare with experiment the quantity (Γ_n/D). This comparison allows one to determine one relation between the real part of the potential and the nuclear radius. Fig. 5 shows the value of (Γ_n/D) for the indicated values of the parameters $V(r)$, r_0, $(1/\alpha)$ and ζ. The maximum of (Γ_n/D) at $A \sim 51$ is evidently displaced to the right

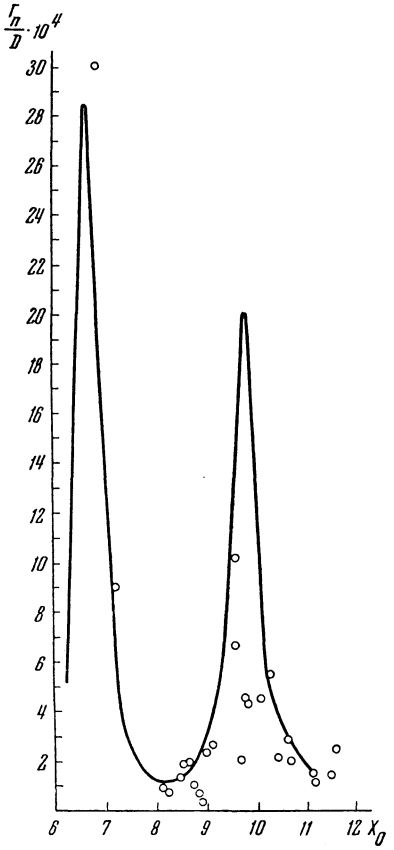

FIG. 5. Ratio of reduced neutron width to level spacing. Parameters $1/\alpha = 0.71 \times 10^{-13}$ cm, $\zeta = 0.05$.

of its theoretical position. But the data are very inaccurate. The height of the maximum does not disagree with the theory. In the region of the minimum at $A \sim 90$–120 the agreement is also satisfactory. The lowering of the second maximum is attributable to non-spherical nuclei. For non-spherical nuclei the position of the maximum is a function of two parameters, the major axis and the eccentricity of the ellipsoid. Since the eccentricity varies abruptly from nucleus to nucleus, the position of exact resonance may never be reached. For $A \sim 200$–230 the experimental values of (Γ_n/D) also agree with the theory.

Nuclei in the range $A = 90$–100 should have some peculiar features. In such nuclei the p-wave maximum should be visible in the cross-sections for forming a compound nucleus even in the energy-region 3–10 kev.

In this region an increase in level density by a factor of 3 or 4 should be observable. There ought to be many weak levels, with neutron widths increasing rapidly with energy like $E^{3/2}$. The observation of these levels seems to lie just at the limit of the resolving power of present-day neutron spectroscopy.

3. SOME CHARACTERISTIC ANGULAR DISTRIBUTIONS

The most interesting angular distributions occur for rather slow neutrons with energies from 0.1 to 0.5 Mev. In this energy-range inelastic scattering is unimportant, and the cross-sections for radiative capture in elements at the middle of the periodic table are small (at 0.5 Mev not greater than 0.2 barn). At these energies, the main interaction of a neutron with nuclei is therefore elastic scattering. The elastic-scattering cross-section σ_s is equal to $\sigma_t - \sigma_r \sim \sigma_t$. However, the angular distribution will be completely different for the two components of σ_t. We have calculated the angular distribution of the optical component with the same values for the parameters as were used in calculating the total cross-section. Figs. 6, 7, 8 show the results for energies 0.11 and 0.44 Mev at $A = 100$ and for energy 0.44 Mev at $A = 84$. In each case the angular distribution is strongly anisotropic. In Fig. 7 there is a peculiar secondary maximum at 180°, which is absent in Fig. 8. Since the calculation of angular distributions of elastic scattering proceeding through compound nucleus formation is not equally reliable, we have nothing to say here about this component. It should be possible to make statements about the compound nucleus component after investigating the distributions in various special cases.

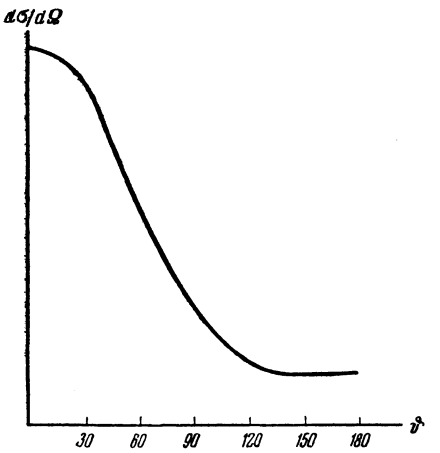

FIG. 6. Angular distribution of optical elastic scattering. Parameters $1/\alpha = 0.71 \times 10^{-13}$ cm, $E = 0.11$ Mev, $A = 100$.

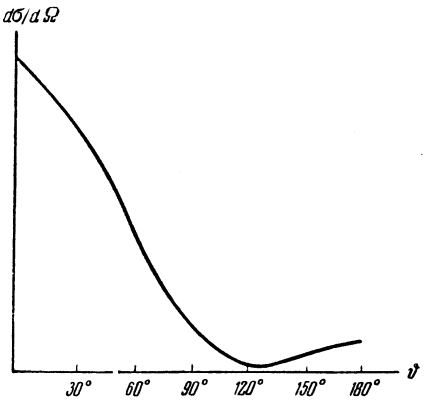

FIG. 7. Angular distribution of optical elastic scattering. Parameters $1/\alpha = 0.71 \times 10^{-13}$ cm, $E = 0.44$ Mev, $A = 100$.

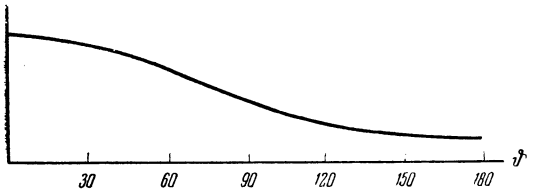

FIG. 8. Angular distribution of optical elastic scattering. Parameters $1/\alpha = 0.71 \times 10^{-13}$ cm, $E = 0.44$ Mev, $A = 84$.

[1] P. E. Nemirovskii, J. Exptl. Theoret. Phys. (U.S.S.R.) **30**, 551 (1956); Soviet Phys. JETP, **3**, 484 (1956).
[2] R. K. Adair, Phys. Rev. **94**, 737 (1954).

Translated by F. J. Dyson
233

SOVIET PHYSICS JETP VOLUME 5, NUMBER 5 DECEMBER, 1957

Contribution to the Theory of the Molecular Generator

IU. L. KLIMONTOVICH AND R. V. KHOKHLOV
Moscow State University

(Submitted to JETP editor June 29, 1956)
J. Exptl. Theoret. Phys. (U.S.S.R.) **32**, 1150-1155 (May, 1957)

Processes of resonance interaction between an electromagnetic field and a molecular beam and also auto-oscillation processes in a molecular generator are examined in the present paper. Unlike other papers, the case of a beam of monochromatic (with respect to velocity) molecules is considered in detail and the peculiarities of this case are elucidated. The result obtained by taking into account non-monochromatic molecules in the beam is discussed qualitatively.

INCREASED STABILITY requirements have led to the development of a molecular generator in which the electromagnetic oscillations in the resonator are excited by radiation of excited gas molecules passing through the resonator. The possibility of such a generator was indicated in 1952 by Basov and Prokhorov[1, 2]. The molecular generator was almost simultaneously developed by a group of American physicists [3, 4] and by Basov and Prokhorov in the U.S.S.R. Even before the experimental success of the molecular generator, Basov and Prokhorov suggested a theory of its operation[5-7], which in essence consists of the following. Using the theory of dispersion, and taking account of saturation effects, the dielectric constant of the molecular beam passing through the resonator is determined. They then examine oscillatory processes in a circuit with a capacitor whose dielectric has the same constant as the molecular beam. The dielectric constant depends on the square of the electric field. Therefore this oscillatory process is described by a non-linear differential equation whose solution determines the amplitudes and frequencies of the oscillation. The theoretical method used by Basov and Prokhorov is not sufficiently complete and makes difficult an analysis of more complicated processes connected with the operation of a molecular generator. We therefore give in the present work a more rigorous statement of the problem, on the basis of which a thorough examination of molecular generator operation in the stationary state is made. We first examine the case of a single-velocity molecular beam ($v = v_0$) and afterwards give a qualitative evaluation of the effect of molecules with speeds other than v_0.

1. In analysis of the operation of a molecular generator it suffices to examine two energetic states